Phys. Status Solidi B **251,** No. 11, 2257–2264 (2014) / **DOI** 10.1002/pssb.201451005

physica status solidi b
www.pss-b.com
basic solid state physics

Unified bandgap engineering of graphene nanoribbons

Vijay K. Arora*[,1,2] and Arkaprava Bhattacharyya[2,3]

[1] Department of Electrical Engineering and Physics, Wilkes University, Wilkes-Barre, PA 18766, USA
[2] Faculty of Electrical Engineering, Universiti Teknologi Malaysia, UTM Skudai 81310, Malaysia
[3] School of Electrical and Electronics Engineering, SASTRA University, Tirumalaisamudram, Thanjavur 613 402, Tamilnadu, India

Received 1 January 2014, revised 10 July 2014, accepted 11 July 2014
Published online 13 August 2014

Keywords band gap, carbon nanotubes, graphene nanoribbons

* Corresponding author: e-mail vijay.arora@wilkes.edu, Phone: +1-570-408-4813, Fax: +1-570-408-7881

Unified bandgap engineering, valid both for the armchair and zigzag graphene nanoribbons (GNRs), is enunciated. Using the boundary condition appropriate for K–K' points of the Dirac cones, GNRs are shown to exhibit three distinct semiconducting states SC0, SC1, and SC2 with complete absence of metallic state. The experimental bandgap for 7-AGNR and 13-AGNR armchair (A) is found to be in excellent agreement with SC1 state. Similar associations are pointed out for other configurations. Both the experimental data and theoretical results show bandgap and effective mass inversely proportional to the GNR width. The effective mass is directly proportional to the bandgap. The indexing scheme connects chiral index of carbon nanotubes (CNTs) to that used for GNR by making edge corrections for the dangling bonds.

1 Introduction Recent experimental sophistications provide various physical and chemical means to materialize graphene nanoribbon (GNR) systems for applications in nanoelectronics of tomorrow. Dutta and Pati [1] review the importance of two different edge geometries, namely zigzag and armchair, arising from the finite termination of graphene, resulting in vast variety of electronic properties of GNR. A number of theories [1] are at odds in predicting the metallic or semiconducting states of a GNR, necessitating transformation of the mindset similar to what has been reported for carbon nanotube (CNT) [2]. The GNR edges are open without any insulator and hence boundary conditions demand antinodes on the edges. The central to all reviewed theories [1] is the band gap and associated effective mass in a semiconducting mode. A cohesive bandgap engineering, similar to what has been reported for a CNT [2] will encourage exploration of ways to enhance its response to external perturbations, doping, and chemical modifications, as well as developing sensors and actuators. Both theory and experiments differ in their outcomes giving metallic or semiconducting GNR depending on the band index similar to what was used for a CNT [2]. The underlying intent of this work is to close that gap in unifying theories that exist in the published literature.

Raza [3] reports the electronic structure of armchair graphene nanoribbons (AGNRs) with periodic edge roughness. The mixed boundary conditions between two Dirac points are shown to result in band-gap opening with and without passivation. Similar boundary conditions between K and K' points in the K-space are utilized to unify the band structure of both zigzag (ZGNR) and armchair (AGNR) nanoribbons. Son et al. [4], based on first-principles approach, present scaling rules for the band gaps of GNRs as a function of their widths. The GNRs considered have either armchair or zigzag shaped edges on both sides with hydrogen passivation. Their *ab initio* calculations show that the origin of energy gaps for GNRs with armchair shaped edges arises from both the quantum confinement and crucial effect of the edges. No empirical relation indicating the bandgap dependence on GNR width is given. CNT being unzipped to form a GNR with standing electron waves is designed [5] in a number of attempts [5, 6]. The electron standing waves are formed similar to sound waves in an open pipe on both ends, as standing waves are restricted to a few-nm width. The spectrum breaks into a set of subbands and electron energy along the confined direction is discretized in terms of bandgap index of the CNT from which it is rolled out into a GNR.

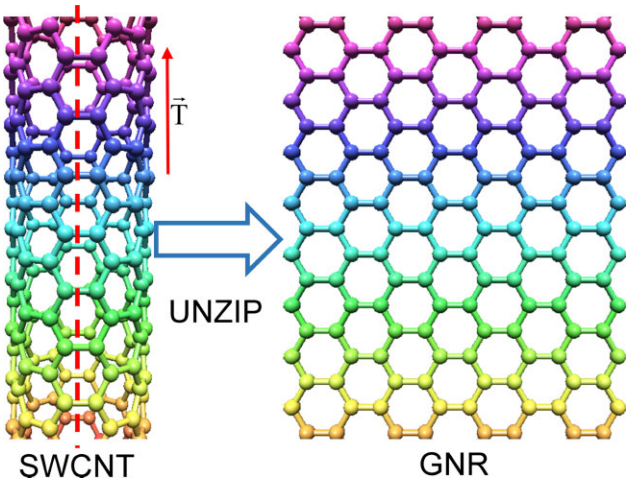

Figure 1 Single-wall armchair carbon nanotube (ACNT) unzipping into a zigzag graphene nano ribbon (GNR).

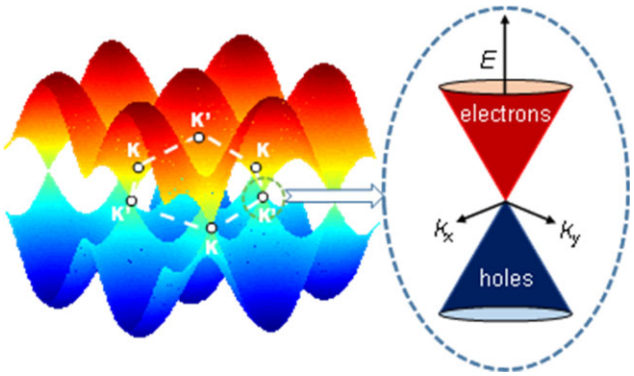

Figure 2 Full-band dispersion from tight-binding approximation over the whole Brillouin zone for π (lower surface or valence band) and π^* (upper surface or conduction band) of graphene. There are $3K$ and $3K'$ points in the Brillouin zone, each K Fermi point residing at the apex of the Dirac cone.

GNR is a cut-out from graphene sheet or rolled out planar nanostructure with narrow width W when CNT is unzipped, as shown in Fig. 1. The example in Fig. 1 is rolled-out ZGNR from an ACNT. The carbon atoms on the edge of GNRs can be both armchair and zigzag shapes, with or without edge extension due to dangling bonds as reported by Raza [3, 7, 8]. Raza and Kan [8] report electronic structure and electric-field modulation calculations in the width direction of AGNRs using a semi-empirical extended Hückel theory. One surprising aspect emerged from this study is absence of metallic AGNR with zero bandgap, indicative of the fact that all bandgaps are semiconducting.

Compared to theoretical landscape predicting the bandgap of GNRs, the experimental measurements of GNR are scant. The most cited is that reported by Han et al. [9]. Their experimental data can be summarized into an empirical relation $E_g = \delta/(W - W^*)$ with $\delta = 0.2$ eV nm and $W^* = 16$ nm attributed to edge effects. No distinction is made between AGNR and ZGNR. Li et al. [10] developed a chemical route to produce GNRs with width below 10 nm, as well as single GNR with varying widths containing lattice-defined graphene junctions for potential molecular electronics. Their experimental data is shown to fit $E_g = \delta/W(\text{nm})$ with $\delta = 0.8$ eV nm. In a most recent study, Chen et al. [11] tuned the bandgap synthesized from covalent self-assembly of new species of molecular precursors. A bandgap of 1.4 eV on 13-AGNR was revealed that is almost a factor of 2 smaller than 2.5 eV experimentally determined on 7-AGNR. These experimental findings have triggered our search for a unified theory that can explain these experimental observations as well as open vista for future experimentation. A unified tactic similar to one reported for CNTs [2] is elucidated in sections to follow.

2 Bandgap engineering The key to bandgap engineering is the 6-K Dirac points of graphene as revealed in Fig. 2. The Dirac cone with linear E–k shape of zero effective mass is a starting point for quantum confinement effect [12]. The K-hexagon is invariant to rotation by $2\pi/6$ about the Γ-point at the center of hexagon with alteration from K to K' or *vice versa* with each segment rotation. This equivalence of K–K' except for the phase is central to the bandgap theory of Dirac fermions in carbon allotropes.

E–k linear relation for a graphene layer is portrayed as

$$E = E_{\text{Fo}} \pm \hbar v_{\text{F}}|k| = E_{\text{Fo}} \pm \hbar v_{\text{F}}\sqrt{k_{\text{L}}^2 + k_{\text{W}}^2}, \qquad (1)$$

where k is the momentum vector with component k_{L} in the longitudinal direction of GNR of length L and width W. k_{W} is the momentum vector component in the direction of width as revealed in Fig. 3. $v_{\text{Fo}} = (1/\hbar)\text{d}E/\text{d}k \approx 10^6$ m/s is the intrinsic Fermi velocity due to linear rise of energy E with momentum vector k. $\hbar v_{\text{Fo}}$is the gradient of E–k dispersion and hence constant. The linear dispersion of Dirac cone is confirmed up to ± 0.6 eV [12]. $E_{\text{F}} - E_{\text{Fo}} = 0$ for intrinsic graphene with $E_{\text{Fo}} = 0$ as the reference level. Here, subscript "o" is added to emphasize the fact that these are intrinsic properties in the metallic state when E–k relation is linear.

A chiral molecule is a type of molecule that has a non-superimposable mirror image. The presence of an asymmetric carbon atom is often the feature that causes chirality in molecules. Chirality is unique to CNTs. CNTs that are superimposable on their mirror image are achiral (not chiral). Those that are *not* superimposable are chiral. Human hands are perhaps the most universally recognized example of chirality: the left hand is a non-superimposable mirror image of the right hand; no matter how the two hands are oriented, it is impossible for all the major features of both hands to coincide. This difference in symmetry is obvious if someone attempts to shake the right hand of a person using his left hand, or if a left-handed glove is placed on a right hand. In mathematics, chirality is the property of a figure that is not identical to its mirror image. In this respect each of AGNR

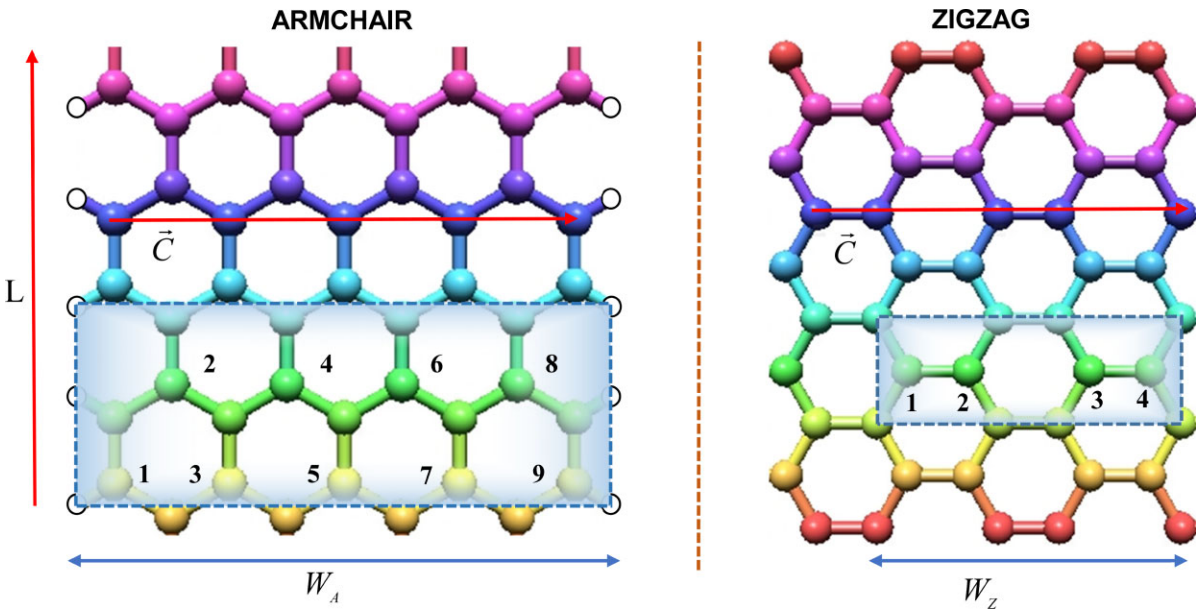

Figure 3 Armchair and zigzag graphene nano ribbons (GNRs) where edges look like armchair and zigzag, respectively, with exemplary chain-index and chiral vector in each case. GNR indexing scheme conforms to p. 68 of Ref. [12].

and ZGNR is achiral as when mirror image of each is present and brought on top of the original will exactly cover it and hence superimposable. GNRs are strips of graphene with ultra-thin width (<50 nm). The electronic states of GNRs largely depend on the edge structures. However, here assumption is made of a perfect edge that has been rolled back from an achiral CNT, thereby width being $W = C \pm \Delta C$, the chiral vector C with corrections ΔC to the dangling bonds at the edges. Chiral vector length derived from CNT with chirality (n,m) giving a GNR is given by [2]

$$C = a\sqrt{n^2 + nm + m^2}, \quad a = \sqrt{3}a_{CC}, \tag{2}$$

where $a = \sqrt{3}a_{CC} = 0.246$ nm is the lattice constant and $a_{CC} = 0.142$ nm is the C–C bond length. As Fig. 3 shows, AGNR is a result of unzipping ZCNT of $(n_A,0)$ chirality. Similarly, ZGNR is a result of unzipping ACNT of (n_Z,n_Z) chirality. Because of high length-to-width aspect ratio, GNRs are 1D nano-conductors. AGNR has an armchair cross-section at the edges. ZGNR has zigzag cross-section. GNRs width (W_A for armchair or W_Z for zigzag) is determined by the number of armchair (N_A) or zigzag (N_Z) chains [12].

Thin, elongated strips of GNR that possess straight edges gradually transform from semiconductors to semimetals as their widths increase and represent a particularly versatile variety of graphene. So, there is naturally a connection between the width W of GNR and chiral vector $C_Z(n_Z,n_Z)$ for zigzag-edged GNR from armchair CNT (n_Z,n_Z) and $C_A(n_A,0)$ for armchair-edged GNR from zigzag CNT $(n_A,0)$. Width of the AGNR and ZGNR is stated in the literature [12] according to number of chains N_A and N_Z as shown in Fig. 3. The other way of describing width is in terms of chiral index. W_A of AGNR is related to chiral length of flattened zigzag CNT (ZCNT) of chirality $(n_A,0)$ and W_Z of ZGNR related to chiral length of the flattened armchair CNT chirality (n_Z,n_Z).

There are two further symmetries of graphene, which are important for understanding CNT being flattened into a GNR. The first is between k and $-k$ states. The second of the two symmetries giving valley degeneracy of $g_K = 2$ can be obtained from Fig. 4 by interchange K and K' points.

In the absence of a magnetic field, forward k and backward $-k$ moving states have identical eigenenergies as is

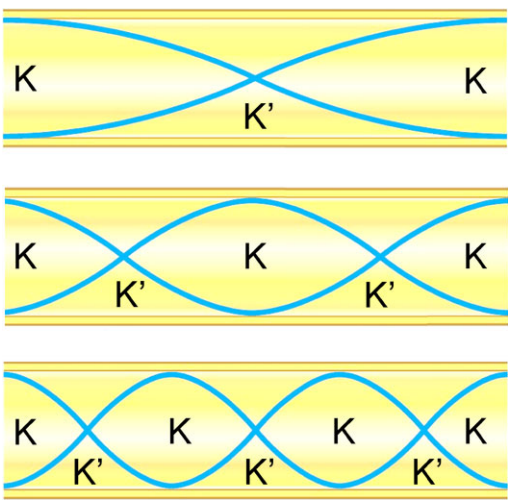

Figure 4 Standing waves in a GNR with different modes. The propagating wave along the width of the tube have phase $k_W W = (2\nu + 1)\pi/6$ as K space is segmented from K to other $3K'$ points. An equivalent pattern is obtained when K and K' are interchanged.

well-known both for parabolic semiconductors as well as for graphene with $E = \hbar v_{\mathrm{Fo}}|k|$. This degeneracy occurs both at K and K' with $\vec{K}' = -\vec{K}$. The total phase change as one starts from a K point and returns to the same in flattened GNR is π. The angular spacing between neighboring K and K' in k-space is $\pi/6$; that between K and next nearest K' is $3\pi/6$; and the furthest is $5\pi/6$ rotating clockwise or counter-clockwise. In general, the phase angle is $(2\nu+1)\pi/6$ where $\nu = 0, 1, 2$. $\nu = 3$ is equivalent to $\nu = 0$ repeating the pattern. The boundary condition for standing waves along the width of GNR is then described as $k_{\mathrm{W}}W = (2\nu+1)\pi/6$ with $\nu = 0, 1$, and 2 with K point into the edges of GNR. The small width of GNRs can lead to quantum confinement of carriers that can be modeled analogous to the standing waves in a pipe open at both ends, as shown in Fig. 4. The first (top) pattern with $\nu = 0$ has $KK'K$ pattern; the middle one has $KK'KK'K$ and the bottom one has $KK'KK'KK'K$. This pattern is degenerate with what is obtained when K and K' are interchanged with K-degeneracy $g_{\mathrm{K}} = 2$. The maximum (antinode) on the open edge can be outside the edge to account for edge effect. That makes effective thickness larger by ΔW, estimated to be around 1.5 nm. This edge effect depends on preparation of the sample on unzipping of a CNT into a GNR. The dispersion for a GNR is now given by

$$E_\nu = E_{\mathrm{Fo}} \pm \hbar v_{\mathrm{Fo}}|k| = E_{\mathrm{Fo}} \pm \hbar v_{\mathrm{Fo}}\sqrt{k_{\mathrm{L}}^2 + \left((2\nu+1)\frac{\pi}{6W}\right)^2}. \quad (3)$$

In terms of bandgap E_{g} around $k_{\mathrm{L}} = 0$, Eq. (3) is written as

$$E_\nu = E_{\mathrm{Fo}} \pm \frac{E_{\mathrm{g}\nu}}{2}\sqrt{1 + \left(\frac{6Wk_{\mathrm{L}}}{\pi(2\nu+1)}\right)^2}. \quad (4)$$

In the parabolic approximation $(k_{\mathrm{L}}W < 1)$, as for a CNT, the bandgap and effective mass are given by

$$E_{\mathrm{g}\nu} = (2\nu+1)\frac{\pi}{3W}\hbar v_{\mathrm{F}} = (2\nu+1)\frac{0.69\,\mathrm{eV\ nm}}{W} \quad (5)$$

and

$$\frac{m^*_{\mathrm{L}\nu}}{m_{\mathrm{o}}} = (2\nu+1)\frac{\pi}{6W}\frac{\hbar}{v_{\mathrm{F}}m_{\mathrm{o}}} = (2\nu+1)\frac{0.06\,\mathrm{nm}}{W}. \quad (6)$$

Figure 5 shows the complete E–k_{L} spectrum with exemplary $N_{\mathrm{A}} = 7$ taken for an AGNR and $N_{\mathrm{Z}} = 8$ for ZGNR. The effective chiral index is $n_{\mathrm{A}} + 1 = 4$ for an AGNR and $n_{\mathrm{Z}} = 4$ for a ZGNR. The bandgap index is $\nu = 1$ in each of these two cases. The linear dotted-dash line passing through the origin in Fig. 4 is the representation of asymptotic behavior as $k_{\mathrm{L}}W \gg 1$. In this extreme, Eq. (4) collapses to

$$E_\nu = E_{\mathrm{Fo}} \pm \hbar v_{\mathrm{Fo}}k_{\mathrm{L}}. \quad (7)$$

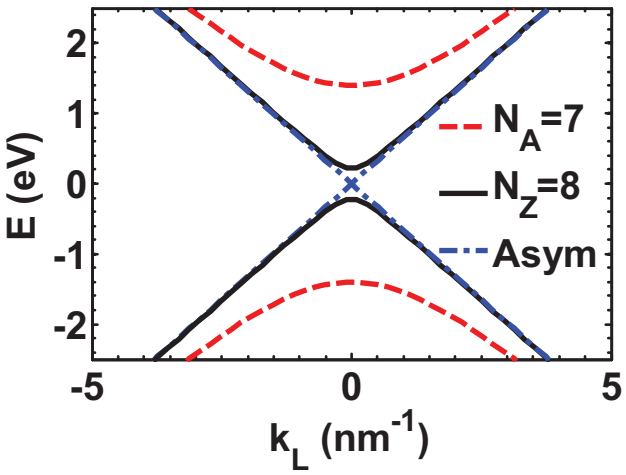

Figure 5 E vs. k_{L} graph for two different armchair and zigzag nanoribbons having similar number of chains ($N_{\mathrm{A}} = 7$ with $n_{\mathrm{A}} + 1 = 4$ and $N_{\mathrm{Z}} = 8$ with $n_{\mathrm{Z}} = 4$) associated with $\nu = 1$. Asymptotic value for large k_{L} is also shown with dotted-dash line.

All E–k_{L} curves are semiconducting in nature with a finite bandgap. The curvature near $k_{\mathrm{L}} = 0$ is parabolic represented by an effective mass. In the large $k_{\mathrm{L}} \to \infty$ limit, the dispersion is linear with Eq. (7) forming an asymptote.

As GNRs are unzipped from CNTs, the width can be related to that of a chiral vector $C_{\mathrm{Z}} = a\sqrt{3}n = 3a_{\mathrm{CC}}n$ for ZGNR unzipped from ACNT. Similarly, $C_{\mathrm{A}} = an = \sqrt{3}a_{\mathrm{CC}}n$ for AGNR unzipped from ZCNT. In this setup, there is no metallic GNR with zero bandgap. The bandgap is a function of the width W with $(2\nu+1) = 1$, 3, or 5 giving three states SC0, SC1, and SC2 and related effective masses $m^*_{\mathrm{L0,1,2}}$.

The bandgap E_{g} as a function of GNR width W is shown in Fig. 6. The experimental data for smaller widths tend to

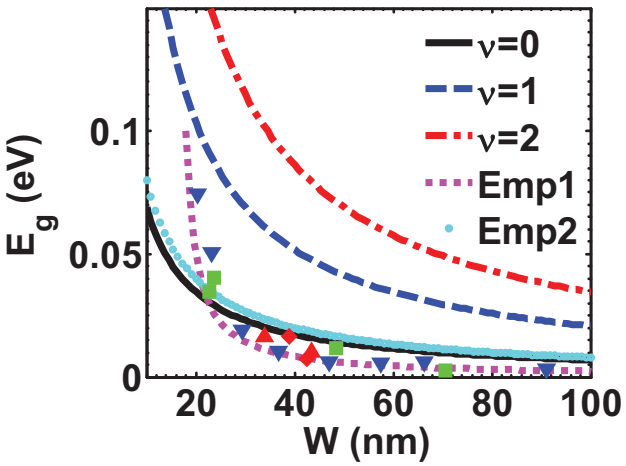

Figure 6 The GNR bandgap as a function of width W. Markers are experimental data (Ref. [9]) with empirical relation marked as Emp1. Also shown is the empirical curve obtained by Li et al. [10] shown as Emp2.

follow $\nu = 2$ curve indicating the transition to $\nu = 1$ as width is increased, ultimately transitioning to $\nu = 0$. GNR transforms to layered graphene for width exceeding 100 nm. The empirical formula for bandgap as a function of width used by Han et al. [9] to fit their experimental data is given by

$$E_g = \frac{\delta}{W - W^*}, \tag{8}$$

with $\delta = 0.2\,\text{eV}$ and $W^* = 16\,\text{nm}$. Equation (8) is represented by the curve indicated "Emp1" in the legend of Fig. 6. The comparison shows that narrower GNRs tend to rise to the curve represented by $\nu = 1$ and $\nu = 2$ indicating the importance of these indices in achieving higher bandgap by engineering GNRs as narrow as $W = 15\,\text{nm}$. Based on the empirical scaling determined, making use of GNRs for semiconducting device components with large bandgap in ambient conditions a possibility by appropriate engineering. Also shown is "Emp2" curve that represents the bandgap relation $E_g = 0.8\,\text{eV nm}/W$ prescribed by Li et al. [10] in fitting their experimental data. They found it difficult to make quantitative comparisons of their extracted band gaps with theory because the precise edge structures of the GNRs are likely to vary between ribbons in various devices with either zigzag, armchair, or mixed edges.

The model presented above predicts bandgap $E_g = \delta/W$ with $\delta = (2\nu + 1)0.69\,\text{eV nm}$. δ can be 0.69 eV for GNR with $\nu = 0$; 2.07 eV with $\nu = 1$; and 3.45 with $\nu = 3$. The values reported for E_g in the literature have wide variations from as low as 0.2 eV and rising to more than 2.0 eV. The periodic symmetry model predicts small bandgap GNR with $\nu = 0$, intermediate bandgap with $\nu = 1$, and large bandgap GNR with $\nu = 2$. Complexity also arises from the nature of GNR (armchair or zigzag). For zigzag GNR (ZGNR), δ and W are found to be the same for all values of N_A, the number of armchair chains. These show ZGNR have a unique value $\nu = 0$ leading to the smallest bandgap. However, for armchair GNR (AGNR), $\nu = 0$, 1, and 2 correspond to three types of semiconducting states.

As one can imagine, the dangling bonds at the surface change the value of E_g and W^* and hence the difficulty of identifying their values uniquely. Another empirical relation cited [12] in the literature is

$$E_g = \frac{\delta}{W + \Delta W}, \tag{9}$$

with $\delta = 0.2 - 1.0\,\text{eV}$ and $\Delta W = 1.5\,\text{nm}$. Ideally $\Delta W = 0$, but the passivation of the edges can make antinode of the standing waves further from the edge of GNR and make ΔW finite.

The effective mass along the length of GNR is shown in Fig. 7. As in CNT, the mass is larger for $\nu = 2$. Once again, as width increases, the electron reaches massless Dirac fermion in a graphene nanolayer.

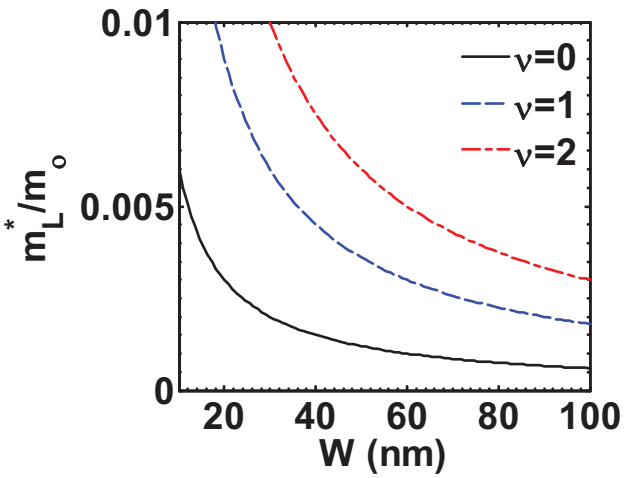

Figure 7 The GNR normalized effective mass as a function of its width for $\nu = 0$, 1, and 2.

The relation between the effective mass and the bandgap is linear and is the same as in a CNT as given by

$$\frac{m_L^*}{m_0} = \frac{E_g}{2m_0 v_{Fo}^2} = \frac{E_g(\text{eV})}{11.37\,\text{eV}} \tag{10}$$

The density of states (DOS) is another important feature that is used for equilibrium [13] and non-equilibrium carrier statistics [14]. The DOS for a GNR follows the same pattern as that for a CNT. The differential DOS $D_{GNR}(E)$, following the same procedure [2] as that for a CNT, is given by

$$D_{GNR}(E) = D_0 \frac{|E|}{\left[E^2 - E_c^2\right]^{1/2}} \tag{11}$$

with

$$D_0 = \frac{4}{\pi\hbar v_F} = 1.93\,\text{nm}^{-1}\,\text{eV}^{-1},\ E_c = \frac{E_g}{2}. \tag{12}$$

Band index ν from energy E is now dropped as it is redundant for a given ν. This DOS is universal for all configurations $\nu = 0$, 1, 2.

3 Armchair GNR The width of AGNR is the adjusted chiral vector C_{ZCNT} of the zigzag CNT (ZCNT), as shown in Fig. 3, giving

$$W_A = C_{ZCNT} + a = n_A a + a = (n_A + 1)a. \tag{13}$$

The additional a in Eq. (13) exists because of dangling bonds that form the armchair and normally not included in the total length in counting the number of chains.

In terms of chain index, W_A is given by [12]

$$W_A = \frac{N_A - 1}{2}a + a, \tag{14}$$

Table 1 Band index, width, bandgap, and effective mass for a number of AGNRs.

number of chains N_A	chiral index $n_A = \frac{N_A-1}{2}$	band index $\nu = (n_A + 1) \bmod 3$	width $W_A = (n_A + 1)a = 0.246(n_A + 1)(\text{nm})$	bandgap E_{gv} (eV)	effective mass m_ν^*/m_0
5	2	0	0.738	0.934	0.082
7	**3**	**1**	**0.984**	**2.104**	**0.185**
9	4	2	1.230	1.683	0.247
11	5	0	1.476	0.467	0.041
13	**6**	**1**	**1.722**	**1.202**	**0.106**
15	7	2	1.968	1.753	0.154
17	8	0	2.214	0.311	0.027
19	9	1	2.460	0.841	0.074
21	10	2	2.706	1.275	0.112

where additional a is added for dangling bonds with length $a/2$ on each side of the GNR.

Equations (13) and (14) yield $n_A = (N_A - 1)/2$, which means $N_A = 3, 5, 7, \ldots$ is an odd number. This nomenclature does not permit the even number of chains for AGNR making comparison difficult with the theoretical framework of Raza and Kan [8]. Table 1 lists a few of the chains for which bandgap and effective mass is calculated. Two points for which experimental results are available are noteworthy [11] and highlighted in Table 1. Chen et al. [11] fine-tuned the bandgap of AGNR with experimental values reported as 2.5 eV for 7-AGNR with $N_A = 7$ and 1.4 eV for 13-AGNR with $N_A = 13$. This is in reasonable agreement with the corresponding predicted values 2.1 and 1.2 eV, considering that the edge effects and stretching/compressing the chains can change the bandgap.

Figure 8 gives the bandgap as a function of width. Circles are the points shown in Table 1. Noteworthy in Fig. 8 is the most recent experimental data of Chen et al. [11] for 7-AGNR and 13-AGNR that follow closely the curve for bandgap index $\nu = 1$ as expected from the corresponding chirality. The local electronic structure of 13-AGNR was characterized by performing measurements on 15 different AGNRs of varying widths from 3 to 11 nm. An asymmetry between the conduction band edge and valence band edge is identified that is not accountable by our theoretical framework. Perhaps that is due to partially filled valence band that causes this asymmetry. In fact, most intrinsic CNTs have been identified to be p-type and certainly that may be the case with GNR, which can be settled by further careful experimentation. This asymmetry is also indicative of the fact that the Fermi energy for a grown GNR is distinct from normally assumed $E_{Fo} = 0$. That is why, we made distinction between E_F and E_{Fo}. The dangling bonds at the edges can add to the carrier concentration and shift the Fermi energy towards to conduction band.

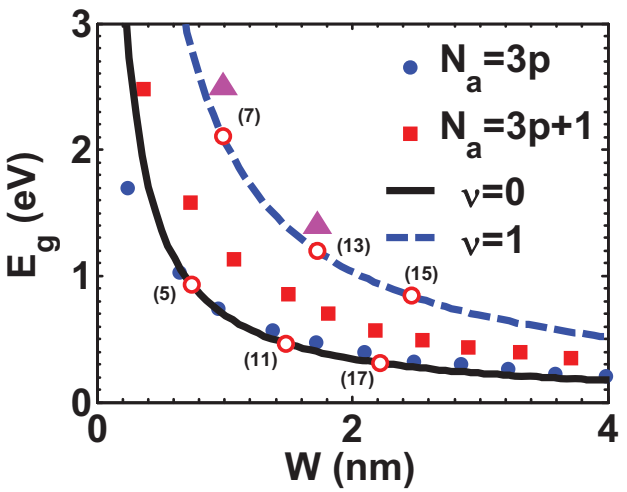

Figure 8 E_g vs. W curve, which compares previous theoretical framework (Son et al. [4]) and band-index based formalism (this work) with two distinct ν values ($\nu = 0, 1$) for AGNRs. Available experimental data ($N_A = 7, 13$) agree well with $\nu = 1$ curve. Open circles in this figure represent data available in Table 1.

Figure 8 also shows the comparison with the theory of Son et al. [4]. Their $N_a = 3p$ and $N_a = 3p + 1$ curves are well replicated by $\nu = 0$ and $\nu = 1$, respectively. In fact, their outcome differs between TB and LDA calculations. In their note added as Ref. [37] in Son et al. [4], it is shown that LDA Kohn–Sham gaps in general underestimate the quasiparticle bandgaps of semiconductors as elucidated by Hybertsen and Louie [15]. They attribute the overall increase in the value of the gap by quasiparticle corrections using the GW approximation as discussed by Miyake and Saito [16]. $N_a = 3p + 2$ mode of predicting small band gap is incompatible with $\nu = 2$ of our framework, confirming that no metallic or small-band-gap state is possible in AGNR. These findings are consistent with the exeprimental data of Chen et al. [11]. giving support to the framework presented.

4 Zigzag GNR Figure 9 shows the bandgap vs. width relation for a zigzag GNR. As CNT is unzipped to form a GNR, the width should be connected to the chiral vector. A ZGNR with zigzag edges is a derivative of armchair CNT (ACNT) of index (n_Z, n_Z). Therefore, the width of ZGNR from the geometry of ACNT is determined to be

$$W_Z = C_{ACNT} - a_{CC} = \sqrt{3}an_Z - a_{CC} = (3n_Z - 1)a_{CC}, \quad (15)$$

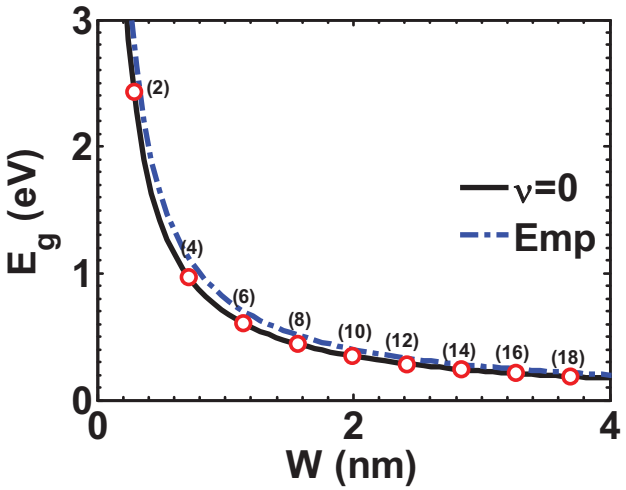

Figure 9 E_g vs. W graph for ZGNR showing with $\nu = 0$. Calculated bandgap as a function of zigzag chain number is shown with open circles. Empirical relation of Li et al. [10] is also shown by blue line.

where a_{CC} is the C–C bond length and $a = \sqrt{3}a_{CC}$ is lattice constant. Subtraction of a_{CC} from C_{ACNT} is necessary to account for extension of C_{ACNT} into edges. In terms of chain index N_Z, the width W_Z is given by [12]

$$W_Z = \frac{3N_Z - 2}{2\sqrt{3}}a = \frac{3N_Z - 2}{2}a_{CC}. \quad (16)$$

Equating (15) to (16) gives $n_Z = N_Z/2$, which means chain index can take only even values $N_Z = 2, 4, 6, ...$

Raza [7] studied ZGNR with periodic roughness and reports significant bandgap opening akin to $\nu = 1$ of AGNR. In fact, he was able to show transitioning of conduction band to valence band with hole-like effective mass with Γ-point bandgap engineering. The periodic edge roughness is a direct amalgamation of ZGNR leading to AGNR as periodic roughness progresses to conditions appropriate for an AGNR. His ball and stick model with $N_A = 8$, 9, and 10 gives conditions intermediate between AGNR and ZGNR, which Li et al. [10] describe as mixed edges.

Raza [7] obtained relation 1.65 eV nm/W(nm) for unified GNR. Open circles correspond to what is calculated in Table 2. Our described formalism thus goes beyond what can be achieved by any of the theories in the specialized domain. The electric-field modulation resulting in triangular quantum well will lead to wave function that can be described by Airy functions as discussed by Fairus and Arora [17], extending the vision of bandgap engineering to uncharted territories. Li et al. [10] are of the opinion that band gaps result from a staggered sublattice potential from magnetic ordering in zigzagged GNRs. The all-semiconductor nature found in their sub-10-nm GNRs is consistent with the band gap opening in GNRs with various edge structures suggested theoretically. Band gap values extracted from the experimental data fall in between the limits of theoretical calculations for zigzag- and armchair-edged GNRs with various widths. Our categorization into various modes with band index ν has made this distinction crisp that makes it easy to interpret the experimental data.

Comparative study of CNT and GNR using similar boundary conditions based on K–K' symmetry indicate that the CNT do show a metallic behavior [2], while GNRs do not. The presence of dangling bonds can increase the line density of electrons and shift the Fermi energy towards conduction band. Relation between GNR and CNT index and chirality can change whether or not the dangling bonds are included. The conduction band edge of 1.21 eV and valence band edge of −0.15 eV determined by Chen et al. [11] shows that intrinsic $E_{Fo} \neq 0$. Hence dangling bonds can also change the symmetry of conduction and valence band. Han et al. [9] did perform a comprehensive experimental measurement in 2007. The closest work to our categorizing the bandgap into three semiconducting states comes from the work of Raza and Kan [8] who have categorized the AGNR bandgap into α, β, and γ categories, based on chain index N_A similar to the categories of Son et al. [4] from first-principles calculations.

5 Conclusions We believe that we have given a comprehensive outlook on the bandgap engineering of GNR to encompass all categories, which will be useful to experimentalists as well as theorists to make comparisons.

Table 2 Band index, width, bandgap, and effective mass for a number of ZGNRs.

number of chains N_Z	chiral index $n_Z = \frac{N_Z}{2}$	band index $\nu = 0$	width $W_Z = (3n_Z - 1)a_{CC} = (3n_Z - 1)0.142$ (nm)	bandgap E_{gv} (eV)	effective mass m^*_ν/m_0
2	1	0	0.284	2.430	0.214
4	2	0	0.710	0.972	0.085
6	3	0	1.136	0.607	0.053
8	4	0	1.562	0.442	0.039
10	5	0	1.988	0.347	0.031
12	6	0	2.414	0.285	0.025
14	7	0	2.840	0.243	0.021
16	8	0	3.266	0.211	0.019
18	9	0	3.692	0.187	0.016

When combined with non-equilibrium Arora distribution function (NEADF) as used for graphene [14], and CNT [18] it can make predictions for both ballistic and quantum transport [14, 18, 19]. Similarly, transformation to bilayer GNR and application to gas sensors can proceed on those lines [20, 21]. Both CNTs and GNRs are also expected to find applications in sensor technology [21]. Complete landscape of graphene folding into CNT and GNR is described in the forthcoming book [22]. Although this reference does not consider the bilayer graphene, the boundary conditions similar to one detailed above for 3D multilayer graphene can yield bandstructure with effective mass similar to what is detailed above. In fact, as discovered above the bandgap from the Dirac point $E_g/2$ is found equivalent to $m^* v_{Fo}^2$ that may open another vista $E = m^* v_{Fo}^2$ similar to the Einstein mass–energy $E = mc^2$ relation based on theory of relativity. This will extend the spectrum of energy–mass relation to embrace Dirac fermions as well. GNRs discussed above and CNTs both follow distinct 1D character with possibility of ballistic quantum resistance similar to what is discussed by Chin et al. [18]. Quantum of resistance $R_Q = h/4q^2 = 6.453\,k\Omega$ is equally perceivable in GNRs, which possess the same K–K' degeneracy provided the length of a GNR is reduced below the ballistic mean free path (mfp) that itself depends on injection from the contacts. Several transport experiments can be designed based on the bandgap engineering noted above, the most crucial one being that in a high electric field that is above its critical value equal to the Fermi voltage $V_F = E_F/q$ divided by mfp. The saturation velocity in a high electric field will be tested by intrinsic velocity that is below the Fermi velocity and also affected by quantum emission. The paradigm presented thus may go a long way in elucidating fundamental physics present in understanding carbaneous materials as future unfolds and carbon expands to mainstream electronics.

Acknowledgements V.K.A. thanks the Universiti Teknologi Malaysia (UTM) for an award of a distinguished visiting professorship and UTM Research University Grant (GUP) Q. J130000.2623.04H32 of the Ministry of Education (MoE). A.B. is a researcher of the Universiti Teknologi Malaysia under the Post-Doctoral Fellowship Scheme.

References

[1] S. Dutta and S. K. Pati, J. Mater. Chem. **20**, 8207 (2010).
[2] V. K. Arora and A. Bhattacharyya, Nanoscale **5**, 10927 (2013).
[3] H. Raza, Phys. Rev. B **84**, 165425 (2011).
[4] Y.-W. Son, M. L. Cohen, and S. G. Louie, Phys. Rev. Lett. **97**, 216803 (2006).
[5] D. V. Kosynkin, A. L. Higginbotham, A. Sinitskii, J. R. Lomeda, A. Dimiev, B. K. Price, and J. M. Tour, Nature **458**, 872 (2009).
[6] H. Santos, L. Chico, and L. Brey, Phys. Rev. Lett. **103**, 086801 (2009).
[7] H. Raza, J. Phys.: Condens. Matter **23**, 382203 (2011).
[8] H. Raza and E. C. Kan, Phys. Rev. B **77**, 245434 (2008).
[9] M. Y. Han, B. Özyilmaz, Y. Zhang, and P. Kim, Phys. Rev. Lett. **98**, 206805 (2007).
[10] X. Li, X. Wang, L. Zhang, S. Lee, and H. Dai, Science **319**, 1229 (2008).
[11] Y.-C. Chen, D. G. de Oteyza, Z. Pedramrazi, C. Chen, F. R. Fischer, and M. F. Crommie, ACS Nano **7**, 6123 (2013).
[12] P. H. S. Wong and D. Akinwande, Carbon Nanotube and Graphene Device Physics (Cambridge University Press, Cambridge, 2011).
[13] R. Qindeel, M. A. Riyadi, M. T. Ahmadi, and V. K. Arora, Curr. Nanosci. **7**, 235 (2011).
[14] V. K. Arora, M. L. P. Tan, and C. Gupta, J. Appl. Phys. **112**, 114330 (2012).
[15] M. S. Hybertsen and S. G. Louie, Phys. Rev. B **34**, 5390 (1986).
[16] T. Miyake and S. Saito, Phys. Rev. B **72**, 073404 (2005). Phys. Rev. B **68**, 155424 (2003).
[17] A. T. M. Fairus and V. K. Arora, Microelectron. J. **32**, 679 (2001).
[18] H. C. Chin, A. Bhattacharyya, and V. K. Arora, Carbon **76**, 451 (2014).
[19] V. K. Arora, D. C. Y. Chek, M. L. P. Tan, and A. M. Hashim, J. Appl. Phys. **108**, 114314 (2010).
[20] E. Akbari, V. Arora, A. Enzevaee, M. Ahmadi, M. Khaledian, and R. Yusof, Plasmonics, in press (2014), doi: 10.1007/s11468-014-9705-4.
[21] E. Akbari, V. K. Arora, M. T. Ahmadi, A. Enzevaee, M. Saeidmanesh, M. Khaledian, H. Karimi, and R. Yusof, Beilstein J. Nanotechnol. **5**, 726–734 (2014).
[22] V. K. Arora, Nanoelectronics: Quantum Engineering of Low-Dimensional Nanoensembles (CRC/Taylor & Francis, Boca Raton, FL, book in press: 2014).

